

Research article

Optimizing Energy Efficiency of Adiabatic Frequency Conversion in an Add-Drop Resonator

Busara Pattanasiri, Werachai Lipar and Santhad Pitakwongsaporn*

Division of Physics, Department of Physical and Material Sciences, Faculty of Liberal Arts and Science, Kasetsart University Kamphaeng Saen Campus, Nakorn Pathom, Thailand

Received: 28 May 2024, Revised: 3 August 2024, Accepted: 4 November 2024, Published: 9 December 2024

Abstract

Adiabatic frequency conversion (AFC) in add-drop resonators holds promise for enhancing energy efficiency in photonic applications. This theoretical study investigates the conditions for optimizing the energy efficiency of the drop port within an add-drop resonator configuration. The analysis considers both fixed input pulse shapes and continuous wave inputs, taking into account AFC's relative timescales. Specifically, the critical coupling regime is explored, and it is observed that the extrinsic decay rates into the drop port and through port converge to nearly equal values, thereby maximizing drop port efficiency. Moreover, when a global parameter is swept, it is demonstrated that the maximal efficiency of the drop port is achieved when the extrinsic decay rates of both ports are equal. This optimization strategy extends to scenarios involving continuous wave inputs as well. These findings provide valuable insights for designing high-performance add-drop resonators and advancing the practical implementation of AFC in photonic systems.

Keywords: adiabatic frequency conversion; add-drop resonators; energy efficiency; photonic applications

1. Introduction

Frequency conversion (FC) plays a crucial role in photonic systems, enabling the manipulation of light signals for diverse applications. Traditionally, nonlinear wave mixing has been the primary method for achieving FC (Lin et al., 2006; Mathlouthi et al., 2008; Breunig, 2016). While this approach has yielded significant advancements, inherent limitations hinder its widespread adoption in integrated photonic circuits (Boyd, 2019). One key challenge associated with nonlinear wave mixing is the requirement for high-power optical pumps. These high pump powers pose a significant barrier to on-chip integration due to increased power consumption and thermal management complexities. Additionally, wave mixing is constrained by the principle of energy conservation, limiting the flexibility of achievable frequency conversions. Finally, achieving efficient wave mixing necessitates careful phase matching between interacting light waves, which can be challenging to maintain across a broad bandwidth.

*Corresponding author: E-mail: faasstpi@ku.ac.th
<https://doi.org/10.55003/cast.2024.263506>

Copyright © 2024 by King Mongkut's Institute of Technology Ladkrabang, Thailand. This is an open access article under the CC BY-NC-ND license (<http://creativecommons.org/licenses/by-nc-nd/4.0/>).

Adiabatic frequency conversion (AFC) has emerged as a promising alternative for manipulating the frequency of light signals. Unlike traditional methods, AFC relies on a unique phenomenon: as light interacts with an optical cavity, the cavity's refractive index is modulated, causing the light to follow the shifting resonance frequency of the cavity itself (Notomi & Mitsugi, 2006). Unlike wave mixing, AFC avoids the need for optical pumping and stringent phase-matching conditions, and it is not limited by photon-energy conservation. AFC has been realized experimentally in several implementations, including photonic crystals (Preble et al., 2007; Tanabe et al., 2009; 2010; Kondo & Baba, 2018), waveguides (Kampfrath et al., 2010; Kondo & Baba, 2014; Fan et al., 2016), structured fiber cavities (Kabakova et al., 2012), integrated lithium niobate resonators using the Pockels effect (Minet et al., 2020), and electrical modulation (He et al., 2022).

Theoretical studies of AFC in optical resonators have explored both its modeling and potential applications in various fields (Daniel et al., 2011a; Xiao et al., 2011; Minkov & Fan, 2018; Shcherbakov et al., 2019). Research has shown that the AFC efficiency for a pulse input in an all-pass resonator can reach 74%, while for an add-drop resonator it is only 18% (Daniel et al., 2011b). While existing research has explored AFC, an important question remains regarding its efficiency in add-drop resonators. In our work, we demonstrate that adiabatic frequency conversion (AFC) of a single pulse can achieve an efficiency of 20%, and for a continuous wave input, the efficiency reaches 25%. This represents a significant improvement over previously reported efficiency. We conducted an extensive theoretical analysis of AFC efficiency in add-drop resonators, thoroughly examining its limitations and identifying the conditions for achieving optimal efficiency. This in-depth analysis of AFC in add-drop resonators is still lacking, making our work a valuable contribution to the field.

By building on the recent development of a coupled-mode theory for analyzing AFC in all-pass resonators (Cortes-Herrera et al., 2022), we present a similar analytical model for achieving optimal AFC in add-drop resonators. Our analysis begins by formulating the governing coupled-mode equations for the system. Using these equations, we derive a general expression for the AFC energy efficiency. Next, we leverage the principles of energy conservation and time-reversibility to identify the critical coupling condition necessary for achieving optimal AFC. To provide a more comprehensive understanding, we subsequently compare the requirements for optimal AFC with pulsed and continuous-wave light inputs. We aim to move AFC beyond theoretical demonstrations and pave the way for practical applications.

2. Materials and Methods

2.1 Analysis of drop port equations

Consider an optical pulse at an angular frequency ω propagating inside a four-port system that consists of a resonator placed between two waveguides depicted in Figure 1. The resonator exhibits evanescent coupling to the waveguides designated as the bus and receiver, respectively. The evolution of the mode's amplitude, denoted by a (where $|a|^2$ represents the mode's energy before modulation), is described by the well-known differential equation (Minkov & Fan, 2018; Shcherbakov et al., 2019; Cortes-Herrera et al., 2022).

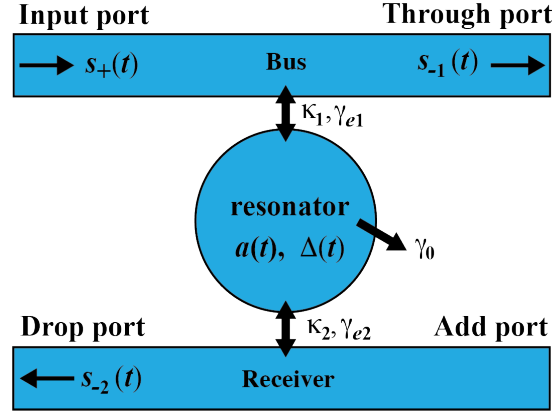


Figure 1. A schematic diagram of the add-drop resonator system used for adiabatic frequency conversion

$$\frac{da}{dt} = -i\Delta(t)a - \gamma a + \kappa_1 s_+(t) \quad (1)$$

Where $\Delta(t) = \omega_c(t) - \omega$ is the detuning from the resonance; $\omega_c(t)$ is the mode's instantaneous frequency; $s_+(t)$ is the incoming wave amplitude, normalized for instantaneous power $|s_+(t)|^2$; κ_1 is a coupling coefficient between the resonator and the bus; and γ is the mode's decay rate, which characterizes how quickly the energy within the resonator diminishes over time. It is the sum of two components: intrinsic decay rate γ_0 and extrinsic decay rate γ_e . The intrinsic decay arises from material absorption and other inherent losses within the resonator. The extrinsic decay γ_e represents the combined effect of coupling losses to the through port γ_{e1} and the drop port γ_{e2} . The overall mode's decay rate is given by (Manolatou et al., 1999):

$$\gamma = \gamma_0 + \gamma_{e1} + \gamma_{e2} \quad (2)$$

In AFC, we can assume that the cavity's resonance frequency is modulated in a step-like manner. This modulation occurs over a timescale significantly shorter than both the half-photon lifetime (γ^{-1}) and the duration of $s_+(t)$. Therefore, $\Delta(t)$ can be labeled as (Cortes-Herrera et al., 2022):

$$\Delta(t) = \Delta_0 H(t - t_0) \quad (3)$$

where t_0 is the modulation time, $H(t)$ the Heaviside function, and Δ_0 the cavity's detuning after modulation.

It was shown by Manolatou et al. (1999) that the appropriate expression for the outgoing waves are

$$s_{-1}(t) = s_+(t)e^{i\phi} + \kappa_1 a(t) \quad (4)$$

$$s_{-2}(t) = \kappa_2 a(t) \quad (5)$$

where ϕ is the phase difference between $s_+(t)$ and $s_{-1}(t)$, and κ_2 is a coupling coefficient between the resonator and the receiver. Due to energy conservation and time-reversibility, the coupling coefficient relates with the respective extrinsic decay rate as (Haus, 1984):

$$\kappa_i = \sqrt{2r_{ei}}, \quad i = 1, 2 \quad (6)$$

As shown in Cortes-Herrera et al. (2022), modulating the cavity causes its resonance frequency to shift. Consequently, the resonator amplitude, $a(t)$, would oscillate at frequency f_0 and then decay over time. The resonator amplitude, $a(t)$, is defined by

$$a(t) = a(t_0)e^{[-(i\Delta_0 + \gamma)(t-t_0)]} \quad (7)$$

The amount of energy U_d transferred to the drop port at the converted frequency can be evaluated using the following expression:

$$\begin{aligned} U_d &= \int_{t_0}^{\infty} dt |s_{-2}(t)|^2 \\ &= \frac{\gamma_{e2}}{\gamma} |a(t_0)|^2 \end{aligned} \quad (8)$$

Since equation (1) depends linearly on $a(t)$, we introduce an auxiliary variable $a_d(t_0)$ for easier analysis.

$$a_d(t_0) = \sqrt{\frac{\gamma_{e2}}{\gamma}} a(t_0) \quad (9)$$

Since $U_d = |a_d(t_0)|^2$, $a_d(t_0)$ can be interpreted as the amplitude of the converted energy, equation (1) can be rewritten in the term of $a_d(t_0)$ as

$$\frac{da_d}{dt_0} = -\gamma a_d + \sqrt{\frac{2\gamma_{e1}\gamma_{e2}}{\gamma}} s_+(t_0) \quad (10)$$

The solution of equation (10) plays a key role in the analysis presented in the following sections.

2.2 Determining the critical coupling regime

If $s_+(t)$ has a $e^{i\omega t}$ time dependence, then we find from equation (1) at steady state

$$a(t) = \frac{\kappa_1 s_+(t)}{i\Delta + (\gamma_0 + \gamma_{e1} + \gamma_{e2})} \quad (11)$$

Substituting $a(t)$ from equation (11) into equation (4), we obtain the reflection from the input port

$$\frac{s_{-1}}{s_{+}} = e^{i\phi} \left[\frac{i\Delta + (\gamma_0 + \gamma_{e1} + \gamma_{e2}) + |\kappa_1|^2 e^{-i\phi}}{i\Delta + (\gamma_0 + \gamma_{e1} + \gamma_{e2})} \right] \quad (12)$$

At resonance

$$\frac{s_{-1}}{s_{+}} = \frac{\gamma_0 - \gamma_{e1} + \gamma_{e2}}{\gamma_0 + \gamma_{e1} + \gamma_{e2}} \quad (13)$$

No reflection is experienced when

$$\gamma_0 + \gamma_{e2} = \gamma_{e1} \quad (14)$$

The power entering the cavity for a given input power $|s_{+}(t)|^2$ is maximized. This is the condition of critical coupling.

2.3 AFC using a fixed input pulse

This section analyzes AFC for fixed-shape input pulse, considering key parameters like decay rates γ_0 , γ_{e1} and γ_{e2} , modulation time t_0 , and pulse duration T_s . To simplify the analysis, we introduce normalized parameters. We define the normalized modulation time $\tau = t_0/T_s$. Additionally, we normalize $s_{+}(t_0)$, which is defined subsequently as

$$s_{+}(t_0) = \frac{\bar{s}_{+}(\tau)}{\sqrt{T_s}} \quad (15)$$

We define a normalized input pulse shape, denoted by $\bar{s}_{+}(\tau)$. This input pulse shape adheres to the normalization

$$\int_{-\infty}^{\infty} d\tau |\bar{s}_{+}(\tau)|^2 = U_s \quad (16)$$

and $|\bar{s}_{+}(\tau)|^2$ is in the order of U_s when $|\tau|$ is less than unity. Substituting equation (15) into equation (10), we obtain

$$\frac{da_d}{d\tau} = -\bar{\gamma}a_d + \bar{\kappa}_2\bar{s}(\tau) \quad (17)$$

Here $\bar{\gamma}$ and $\bar{\kappa}_2$ are the normalized decay rate and coupling coefficient between the resonator and the receiver, respectively. These are defined as

$$\bar{\gamma} \equiv (\gamma_0 + \gamma_{e1} + \gamma_{e2})T_s \quad (18)$$

$$\bar{\kappa}_2 \equiv \sqrt{\frac{2\gamma_{e1}\gamma_{e2}}{\bar{\gamma}}} T_s \quad (19)$$

To analyze the impact of input pulse on AFC efficiency for the drop port, we consider a raised cosine pulse. This type of pulse has a non-zero value within $|\tau| < \tau_0$. It can be described by the equation

$$\bar{s}_+(\tau) = \sqrt{\frac{8U_s}{3}} \cos^2(\pi\tau) [H(\tau + \tau_0) - H(\tau - \tau_0)] \quad (20)$$

The raised cosine function depicted in equation (20) is also known as the Hann window function.

To investigate how the AFC energy efficiency η of the drop port is affected by the system's timescales, we perform a numerical analysis. This involves sweeping the normalized timescales of the process and solving equation (17) for their corresponding values and the raised-cosine input shape $\bar{s}_+(\tau)$ of equation (20). These normalized parameters, t_0/T_s , $\gamma_0 T_s$, $\gamma_{e1} T_s$, and $\gamma_{e2} T_s$, define a four-dimensional space. First, we perform three parameter sweeps while keeping one parameter fixed to identify the optimum values for all parameters. We consider the critical coupling regime ($\gamma_{e1} = \gamma_0 + \gamma_{e2}$) and fix the pulse width ($\gamma_0 T_s = 1$). To facilitate visualization and focus on optimization, we reduce the dimensionality of the parameter space in these sweeps by considering only the optimum η over the normalized parameters γ_{e2} and γ_{e1} , respectively. Then, we conduct a global parameter sweep, where all four normalized parameters are varied simultaneously to find the optimum values. For visualization purposes, we again reduce the dimensionality by setting $\gamma_{1e} = \gamma_{2e}$ and considering only the optimum η over the normalized modulation time t_0/T_s .

2.4 AFC using a continuous-wave (cw) input

This section focuses on AFC with a continuous-wave (CW) input of constant power P , which turns on at $t = 0$ with a negligible rise time compared to the resonator's decay rates. Under these conditions, the input field $s_+(t)$ in equation (10) can be written as

$$s_+(t) = (P)^{1/2} H(t) \quad (21)$$

Using this expression for $s_+(t)$, we can solve equation (10) for $a_d(t_0)$ in closed form. The solution, considering the maximum possible converted energy U_d^{max} as defined in Cortes-Herrera et al. (2022), ($U_d^{max} = \frac{8P}{27\gamma_0}$), is given by

$$U_d = \frac{27\gamma_{e1}\gamma_{e2}\gamma_0}{4\gamma^3} U_d^{max} (1 - e^{-\gamma t_0}) \quad (22)$$

Unlike the fixed input pulse case, the cw input in equation (21) has infinite energy U_s . This prevents us from normalizing U_d relative to U_s . However, normalizing U_d is still useful. It enables us to perform a general parameter sweep that explores the ratios of γ_{e1}/γ_0 , γ_{e2}/γ_0 , and modulation timescales $\gamma_0 t_0$ instead of their absolute values. Therefore, we focus on the cw efficiency $\eta_{cw} \equiv U_d/U_d^{max}$. For visualization, we again reduce the dimensionality by considering only the optimum η over the parameter γ_{e1}/γ_0 .

3. Results and Discussion

After defining $\bar{s}_+(\tau)$ in equation (20), we explore how different parameter values affect the solution $a_d(\tau)$ of equation (10). We then calculate the corresponding drop port energy efficiency η using $\eta = U_d/U_s$. To efficiently explore a wide range of parameter combinations, we use logarithmic scales for the parameters. Additionally, since we are primarily interested in maximizing the delivered energy U_d , which depends on the squared magnitude of $|a_d(\tau)|^2$ by considering only the range of $\tau = t_0/T_s$ between $-1/5$ and $-1/2$.

Figure 2 presents the results of our initial parameter sweep. We fix the resonator at critical coupling ($\gamma_0 + \gamma_{e2} = \gamma_{e1}$) and explore a range of t_0/T_s and $\gamma_0 T_s$ while keeping the optimal γ_{e2} at $40.4503\gamma_0$. This figure essentially visualizes energy efficiency η for various combinations of modulation times t_0 and pulse durations T_s with fixed γ_0 and γ_{e1} . A key feature of Figure 2 is the maximum of η at $\gamma_0 T_s = 0.0289$ and $t_0/T_s = 0.2189$, where η reaches a value of 0.1940. This implies that for critical coupling, maximizing efficiency requires setting the pulse duration T_s to $0.0289\gamma_0^{-1}$ and the modulation time t_0 to $0.2189T_s$. The drop port efficiency here ($\eta = 0.1940$) is significantly lower than the 0.7951 achieved in the through port of an all-pass resonator (Cortes-Herrera et al., 2022). This is because the add-drop resonator splits its output power between two ports. However, the efficiency reduction is not simply halved but quartered in this case. The reason for this additional factor of 2 is that, for the same mode decay rate, the add-drop resonator requires twice the input power coupling strength compared to an all-pass resonator. This stronger coupling ensures the same amount of pulse energy enters the resonator, leading to the additional efficiency decrease by a factor of two. The red dashed line in Figure 2 shows that for a given value of $\gamma_0 T_s$, the modulation time t_0 for maximum η monotonically decreases with increasing $\gamma_0 T_s$.

Figure 3 presents the results of another parameter sweep. Here, we fix the normalized pulse width $\gamma_0 T_s$ at 1 and explore a range of t_0/T_s and γ_{e2}/γ_0 while keeping the optimal $\gamma_{e1} = 2.1816\gamma_0$. In simpler terms, we fix the intrinsic decay rate γ_0 and the pulse duration T_s , but vary the modulation time t_0 and the external decay rate γ_{e2} . Similar to Figure 2, we identify a combination of parameters that maximizes the drop port AFC efficiency η , which reaches a peak value of 0.1093. This maximum efficiency occurs at $\gamma_{e2} = 2.1910\gamma_0$ and $t_0 = 0.1416T_s$. The relatively low peak efficiency ($\eta = 0.1093$) suggests that setting $\gamma_0 T_s = 1$ is not ideal for maximizing the drop port efficiency. Interestingly, the red dashed line again shows that the modulation time t_0 for optimal efficiency decreases as the normalized external decay rate γ_{e2}/γ_0 increases. This behavior can be understood by considering the function $a_d(\tau)$ as the output of a low-pass filter.

As shown in Figure 4, a comprehensive parameter sweep was conducted. In this sweep, we explored the entire parameter space by simultaneously varying all normalized parameters: t_0/T_s , $\gamma_0 T_s$, γ_{e1}/γ_0 , and γ_{e2}/γ_0 . We found that the maximum efficiency η occurs at $t_0 = 0.2172T_s$ and $\gamma_{e1} = \gamma_{e2}$. To address this dependence, we eliminate the dependence of η on t_0 and γ_{e1} by plotting only the maximum values of η over t_0/T_s and $\gamma_{e1} = \gamma_{e2}$ for each pair of values of $\gamma_0 T_s$ and γ_{e2}/γ_0 . As is evident from Figure 4, a necessary condition for maximizing η is to minimize $\gamma_0 T_s$. Furthermore, as $\gamma_0 T_s$ approaches 0, the optimal γ_{e2} that maximizes η for a given $\gamma_0 T_s$ (red dashed line) converges to the asymptote

$$\gamma_{e2} T_s = 1.1891, \quad \gamma_0 T_s \ll 1 \quad (23)$$

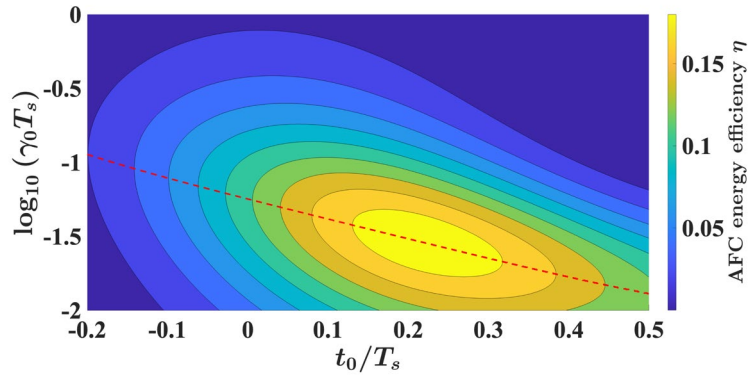


Figure 2. Contour plot of drop port AFC energy efficiency η for Hann pulse in the case of critical coupling ($\gamma_0 + \gamma_{e2} = \gamma_{e1}$)

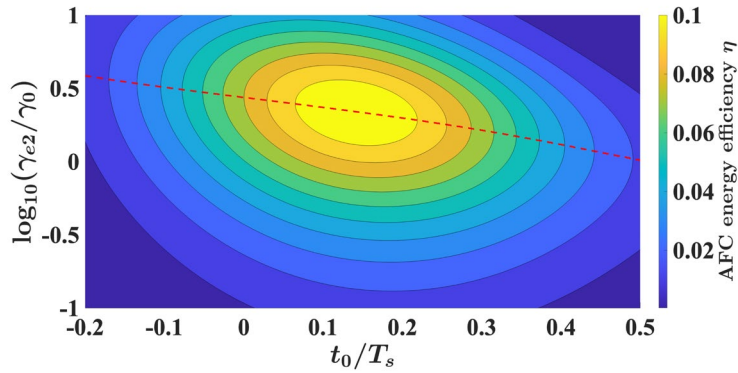


Figure 3. Contour plot of drop port AFC energy efficiency η for Hann pulse in the case of a fixed value of the normalized pulse duration ($\gamma_0 T_s = 1$)

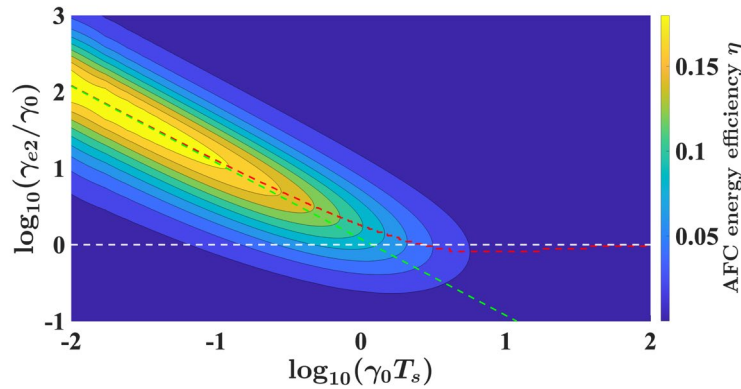


Figure 4. A global sweep in this figure explores the impact of normalized pulse duration $\gamma_0 T_s$ and external decay γ_{e2}/γ_0 on the drop port AFC efficiency of a Hann pulse. The sweep considers modulation time t_0 optimization, resulting in γ_{e1} being set equal to γ_{e2} .

Equation (23) corresponds to the straight line $\log_{10}(\gamma_{e2}/\gamma_0) = \log_{10}(1.1891) - \log_{10}(\gamma_0 T_s)$ depicted graphically as a green dashed line. To understand how equation (23) emerges, we consider the idealized case of a resonator with no intrinsic loss ($\gamma_0 = 0$). It follows from equations (18) and (19): $\bar{\gamma} = \gamma_{e1} T_s + \gamma_{e2} T_s$ and $\bar{\kappa}_2 = \sqrt{2\gamma_{e1}\gamma_{e2} T_s / \bar{\gamma}}$, respectively. As a result, η depends only on t_0/T_s , $\gamma_{e1} T_s$, and $\gamma_{e2} T_s$. To visualize this idealized case, we found that the optimal energy efficiency is achieved at $\gamma_{e1} T_s = 1.1877$. We then explored a range of t_0/T_s and $\gamma_{e2} T_s$. We found that η is maximized at $t_0/T_s = 0.2196$ and $\gamma_{e2} T_s = 1.1877$, which matches γ_{e1} , achieving a value of $\eta = 0.1988$.

As $\gamma_0 T_s$ approaches unity, the external coupling γ_{e2} required for maximum η progressively deviates from equation (23). When $\gamma_0 T_s$ exceeds unity, the γ_{e2} required to maximize η is no longer accurately described by equation (23). Instead, the optimal γ_{e2} converges to the asymptote

$$2\gamma_{e2} = \gamma_{e1} + \gamma_0 \quad (24)$$

To understand the origin of equation (24): if $\gamma_0 T_s \gg 1$, then $\bar{\gamma}^{-1} \ll 1$. Consequently, the differential equation (10) reduces to the algebraic relation

$$a_d = \frac{\bar{\kappa}_2}{\bar{\gamma}} s_+(\tau) \quad (25)$$

Maximizing the converted energy U_d requires maximizing the coefficient $\bar{\kappa}_2 \bar{\gamma}^{-1}$ with respect to the γ_{e2} . Equation (24) expresses this optimization for $\bar{\kappa}_2 \bar{\gamma}^{-1}$. Notably, equation (24) is independent of the input pulse shape.

Figure 5 shows the global parameter sweep for optimizing the drop port AFC energy efficiency η_{cw} for cw input. We again find that to maximize η_{cw} , γ_{e1} must equal γ_{e2} . Therefore, we reduce the parameter space by plotting only the maximum η_{cw} over γ_{e1}/γ_0 for each pair of values for $\gamma_0 t_0$ and γ_{e2}/γ_0 . At the maximum η_{cw} , we find $\gamma_0 t_0 = 12.4901$, $\gamma_{e1} = \gamma_{e2} = 0.9993\gamma_0$, and η_{cw} reaches 0.2500. Similarly to Figure 4, the red dashed line represents the curve corresponding to the values of γ_{e2} that optimize η_{cw} for a fixed $\gamma_0 t_0$ in Figure 5. For $\gamma_0 t_0 \gg 1$, this curve asymptotically follows equation (24), depicted as a white dashed line in Figure 5. Besides, there is a different asymptote for $\gamma_0 t_0 \ll 1$, represented by the curve

$$\gamma_{e2} t_0 = 0.6286, \quad \gamma_0 t_0 \ll 1 \quad (26)$$

To determine the value of 0.6286 in equation (26), we consider equation (22) for $\gamma_0 = 0$ and numerically optimize the resulting expression for U_d with respect to $\gamma_{e1} t_0$ and $\gamma_{e2} t_0$. The straight line corresponding to equation (26) is shown as a green dashed line in Figure 5.

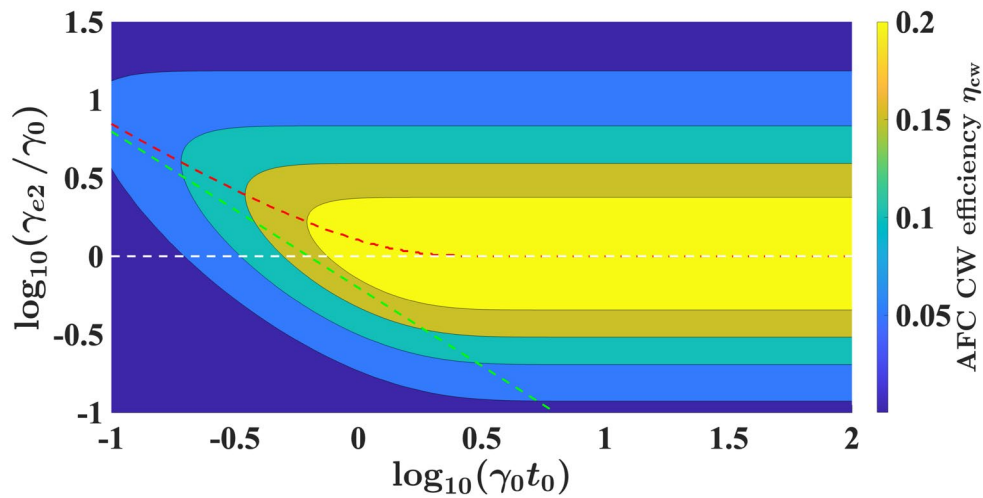


Figure 5. Contour plot of drop port AFC energy efficiency η_{cw} for a cw input

4. Conclusions

This paper presents a thorough theoretical analysis of the maximum energy efficiency achievable at the drop port during adiabatic frequency conversion in an add-drop resonator. We studied how the efficiency of adiabatic frequency conversion (AFC) is affected by the different timescales within a fixed input pulse. We found that the drop port amplitude of the AFC behaves like a low-pass filtered signal, and that for optimal AFC efficiency, the extrinsic dissipation at the drop port and the through port need to be very close to each other. Following this, we investigated the AFC's behavior when a continuous-wave (CW) optical signal is used as the input. We again found that maximum drop port energy is achieved when the extrinsic dissipation at both the drop port and the through port are equal. Optimizing extrinsic dissipation in this manner is beneficial for all AFC implementations in add-drop resonators.

5. Conflicts of Interest

The authors declare that they have no conflicts of interest.

References

- Boyd, R.W. (2019). *Nonlinear Optics* (3rd ed.). Academic Press.
- Breunig, I. (2016). Three-wave mixing in whispering gallery resonators. *Laser & Photonics Reviews*, 10(4), 569-587. <https://doi.org/10.1002/lpor.201600038>
- Cortes-Herrera, L., He, X., Cardenas, J., & Agrawal, G. P. (2022). Optimization of adiabatic frequency conversion in an all-pass resonator. *Physical Review A*, 106, Article 023517. <https://doi.org/10.1103/PhysRevA.106.023517>
- Daniel, B. A., Maywar, D. N., & Agrawal, G. P. (2011a). Dynamic mode theory of optical resonators undergoing refractive index changes. *Journal of the Optical Society of America B*, 28(9), 2207-2215. <https://doi.org/10.1364/JOSAB.28.002207>

- Daniel, B. A., Maywar, D. N., & Agrawal, G. P. (2011b). Efficient adiabatic wavelength conversion in Gires-Tournois resonators. *Optics Letters*, 36(21), 4155-4157. <https://doi.org/10.1364/OL.36.004155>
- Fan, L., Zou, C.-L., Poot, M., Cheng, R., Guo, X., Han, X., & Tang, H. X. (2016). Integrated optomechanical single-photon frequency shifter. *Nature Photonics*, 10(12), 766-770. <https://doi.org/10.1038/nphoton.2016.206>
- Haus, H. A. (1984). *Waves and fields in optoelectronics*. Prentice Hall.
- He, X., Cortes-Herrera, L., Opong-Mensah, K., Zhang, Y., Song, M., Agrawal, G. P., & Cardenas, J. (2022). Electrically induced adiabatic frequency conversion in an integrated lithium niobate ring resonator. *Optics Letters*, 47(22), 5849-5852. <https://doi.org/10.1364/OL.473113>
- Kabakova, I. V., Yu, Z., Halliwell, D., Fonjallaz, P. Y., Tarasenko, O., de Sterke, C. M., & Margulis, W. (2012). Switching and dynamic wavelength conversion in a fiber grating cavity. *Journal of the Optical Society of America B*, 29(1), 155-160. <https://doi.org/10.1364/JOSAB.29.000155>
- Kampfrath, T., Beggs, D. M., White, T. P., Melloni, A., Krauss, T. F., & Kuipers, L. (2010). Ultrafast adiabatic manipulation of slow light in a photonic crystal. *Physical Reviews A*, 81(4), Article 043837. <https://doi.org/10.1103/PhysRevA.81.043837>
- Kondo, K., & Baba, T. (2014). Dynamic wavelength conversion in copropagating slow-light pulses. *Physical Review Letters*, 112(22), Article 223904. <https://doi.org/10.1103/PhysRevLett.112.223904>
- Kondo, K., & Baba, T. (2018). Adiabatic wavelength redshift by dynamic carrier depletion using p-i-n diode-loaded photonic crystal waveguides. *Physical Reviews A*, 97(3), Article 033818. <https://doi.org/10.1103/PhysRevA.97.033818>
- Lin, Q., Zhang, P., Fauchet, M., & Agrawal, G. P. (2006). Ultrabroadband parametric generation and wavelength conversion in silicon waveguides. *Optics Express*, 14(11), Article 4786. <https://doi.org/10.1364/OE.14.004786>
- Manolatou, C., Khan, M. J., Fan, S., Villeneuve, P. R., & Haus, H. A. (1999). Coupling of modes analysis of resonant channel add-drop filter. *IEEE Journal of Quantum Electronics*, 35(9), 1322-1331.
- Mathlouthi, W., Rong, H., & Paniccia, M. (2008). Characterization of efficient wavelength conversion by four-wave mixing in submicron silicon waveguides. *Optics Express*, 16, Article 16735. <https://doi.org/10.1364/OE.16.016735>
- Minet, Y., Reis, L., Szabados, J., Werner, C. S., Zappe, H., Buse, K., & Breunig, I. (2020). Pockels-effect-based adiabatic frequency conversion in ultrahigh-Q microresonators. *Optics Express*, 28(3), 2939-2947. <https://doi.org/10.1364/OE.378112>
- Minkov, M., & Fan, S. (2018). Localization and time-reversal of light through dynamic modulation. *Physical Reviews B*, 97(6), Article 060301(R). <https://doi.org/10.1103/PhysRevB.97.060301>
- Notomi, M., & Mitsugi, S. (2006). Wavelength conversion via dynamic refractive index tuning of a cavity. *Physical Reviews A*, 73(5), Article 051803. <https://doi.org/10.1103/PhysRevA.73.051803>
- Preble, S. F., Xu, Q., & Lipson, M. (2007). Changing the colour of light in a silicon resonator. *Nature Photonics*, 1(5), 293-296.
- Shcherbakov, M. R., Shafrin, P., & Shvets, G. (2019). Overcoming the efficiency-bandwidth tradeoff for optical harmonics generation using nonlinear time-variant resonators. *Physical Reviews A*, 100(6), Article 063847. <https://doi.org/10.1103/PhysRevA.100.063847>
- Tanabe, T., Kuramochi, E., Taniyama, H., & Notomi, M. (2010). Electro-optic adiabatic wavelength shifting and Q switching demonstrated using a p-i-n integrated photonic crystal nanocavity. *Optics Letters*, 35(23), 3895-3897. <https://doi.org/10.1364/OL.35.003895>

- Tanabe, T., Notomi, M., Taniyama, H., & Kuramochi, E. (2009). Dynamic release of trapped light from an ultrahigh-Q nanocavity via adiabatic frequency tuning. *Physical Review Letters*, 102(4), Article 043907. <https://doi.org/10.1103/PhysRevLett.102.043907>
- Xiao, Y., Maywar, D. N., & Agrawal, G. P. (2011). Optical pulse propagation in dynamic Fabry-Perot resonators. *Journal of the Optical Society of America B*, 28(7), 1685-1692. <https://doi.org/10.1364/JOSAB.28.001685>